World Journal of Advanced Engineering Technology and Sciences

eISSN: 2582-8266

Cross Ref DOI: 10.30574/wjaets

Journal homepage: https://wjaets.com/

(RESEARCH ARTICLE)

Check for updates

Enhanced hydrogen production through visible light photocatalysis using 2D MoS_2/2D CdS composite

Pinque, Marbert D and de Leon, Rizalinda L *

Fuels, Energy & Thermal Systems Laboratory, Department of Chemical Engineering, University of the Philippines Diliman, Quezon City 1101, Philippines.

World Journal of Advanced Engineering Technology and Sciences, 2023, 08(01), 352–365

Publication history: Received on 16 January 2023; revised on 22 February 2023; accepted on 25 February 2023

Article DOI: https://doi.org/10.30574/wjaets.2023.8.1.0066

Abstract

This study seeks to enhance the morphological face contact between 2D molybdenum disulfide (MoS_2) nanosheets containing 1T and 2H phases (inhomogeneous) and 2D cadmium sulfide (CdS) sheets/flakes for enhanced charge transfer. The sulfides are synthesized by hydrothermal and solvothermal methods, respectively. MoS_2/CdS composites (5, 10, 15, 20, 25 wt.% MoS_2) are prepared using a physical method. The 2D forms and compositions of both materials are confirmed by FE-SEM imaging, XRD patterns, and XRF semi-quantitative analysis. XRD patterns also reveal the presence of 1T and 2H phases in MoS_2 as well as the similar morphological and crystalline structures of the two sulfides. The adsorption of MoS_2 onto the CdS surface has minimal intervention of the latter's lattice structure as indicated by UV-Vis diffuse reflectance spectroscopy. A hydrogen production rate of 1036.1 μmol g_{cat}^{-1} h^{-1} is observed using the 15 wt.% MoS_2/CdS composite which was 159 times larger than bare CdS, with photocatalytic retention of about 80 % after 15 hours of use.

Keywords: Hydrogen production; Photocatalysis; 2D-2D; Molybdenum disulfide; Cadmium sulfide

1. Introduction

Pressing issues on global warming mitigation have been a never-ending topic of global environmental agenda and social protests for years. The main anthropogenic factor of climate change is the greenhouse gases (GHGs) emissions from the transportation and power sectors. The dream is to attain zero net anthropogenic emission before the century ends which can be achieved presently by carbon-capture-and-storage technologies, bioenergy production, and/or exploration of viable renewable energy sources. One of the most promising paths in renewable energy is by converting solar energy to chemical energy in a form of hydrogen molecule from water. Hydrogen has exceptional advantages over traditional fossil fuels such as clean combustion, flexible storage options, abundance of sources, and higher heating values [1]. Production of hydrogen can come from electrolysis, thermolysis, thermochemical processes, photovoltaic electrolysis, photocatalysis, and photoelectrolysis [2]. Among these methods, photocatalysis is the most desirable due to its low Global Warming Potential and Acidification Potential [2].

Photocatalytic hydrogen production via water splitting involves dissociation of water into hydrogen and oxygen triggered by photoexcitation of electrons in the photocatalyst. The free energy of this reaction is 238 kJ/mol which corresponds to a potential difference of 1.23 eV. This is the minimum amount of energy which the photoexcitation of electrons from the valence band to the conduction band (band gap energy) of the photocatalyst must overcome. In addition, the conduction band minimum of the photocatalyst must be more negative than the hydrogen reduction potential to yield hydrogen molecules spontaneously and on the other side, the valence band must be more positive than the water oxidation potential. Aside from the potential difference of 1.23 eV, several activation barriers from

* Corresponding author: de Leon, Rizalinda L

energy losses exist during the reaction which will incur additional energy requirement [3]. A photocatalyst with a band gap energy greater than 1.23 eV is therefore desired. However, too wide a band gap is not desirable to utilize visible light irradiation which comprises a large portion (*ca.* 46%) of sunlight irradiation as the source of photons. In the visible spectrum, the maximum energy is around 380 nm or 3.10 eV. An ideal base-material photocatalyst then for water splitting under visible light irradiation must have a band gap narrower than 3.10 eV.

Ever since Fujishima and Honda realized the photoelectrochemical activity of titanium dioxide (TiO_2) for water splitting, several semiconductor-based photocatalysts (*e.g.*, ZnO, CdS, UV-active oxides) were used in studies for photocatalytic hydrogen evolution as an approach in solving world energy crisis [4]. TiO_2 could have been a promising photocatalyst because of its non-toxicity, physical and chemical stability, except for its band gap of around 3.20 eV so it could only make use of energy from the ultraviolet region which only comprises 5% of solar irradiation [5,6]. Different materials have their own lapses in their performances. In the case of Cadmium sulfide (CdS), it is a promising photoactive material that can utilize energy from the visible light region for water splitting due to its relatively low band gap (2.4 eV) and suitable band gap positions. However, this material exhibits hindrances to its activity such as photocorrosion and rapid electron-hole pair recombination [7]. To suppress recombination of the electron-hole pair several techniques were done such as metal ion doping and combining with other materials (cocatalysts) forming heterostructures [8-11]. These heterostructures are designed to modify the bandgap and its alignment to increase the rate of charge transfer (*e.g.*, electrical conductivity) of semiconductors.

Several cocatalysts have been reported in successfully enhancing the activity of CdS by promoting hydrogen evolution which are usually noble metals such as platinum and gold due to their hydrogen adsorption capacity. A group of materials called layered transition-metal dichalcogenides (TMDs), an analogue of graphene, exhibit diverse promising properties and applications such as in energy storage, catalysis, and opto-electronics [12]. Specifically for hydrogen evolution reaction (HER) applications, molybdenum disulfide (MoS_2) has been attracting research interests for years due to its comparable performance with the costly platinum from electrochemical and photocatalytic tests [13,14].

MoS_2 is an excellent cocatalyst that can form heterojunctions with photoactive materials or semiconductors such as CdS, TiO_2, and reduced graphene. Specifically, MoS_2 and CdS are compatible materials for a composite since they can both have hexagonal crystalline structures enhancing the charge transfer from photoexcitation and have a band alignment (*i.e.*, straddling gap type) suitable for water splitting [15,16]. Two-dimensional (2D) materials are promising candidates in photocatalytic applications because of their high surface area, superior electron mobility, and abundant surface active sites [17]. MoS_2 nanosheets (2D) from incomplete intercalation produces two phase coordination namely: 1T phase which is metallic and highly conductive but metastable and 2H phase which is semiconductive and stable [14]. The presence of these phases in MoS_2 nanosheets is expected to have a synergistic effect in terms of HER enhancement caused by increased number of active sites by 1T phase and stability by 2H phase. Moreover, combining two 2D layered materials provides enhancement of photocatalytic performance due to their architectural stability and increase in contact area which improves charge transfer rate in comparison with other dimensional combinations [17]. It is therefore expected that the heterojunction formation of 2D CdS (photocatalyst) and 2D MoS_2 (cocatalyst) can form large 2D interfaces that will hugely enhance photo-induced charge transfer.

Two 2D-2D MoS_2/CdS photocatalysts were studied by the groups of Yuan and of Ma in colloidal and visible-light driven reactions which confirmed the enhancement of photocatalytic activities of MoS_2/CdS composites due to the formation of heterojunction or 2D interface that promotes faster charge separation [18,19]. However, their works utilized 2H-MoS_2 only.

In this work, 2D MoS_2 from incomplete intercalation, containing both 1T and 2H phases, is used as a cocatalyst for CdS. A heterojunction is formed between MoS_2 nanosheets and CdS sheets via physical force and as a result, a superior photocatalytic performance of the 2D-2D composite was observed compared to the individual material's activities. An apparent synergistic effect of the two materials was observed with 159-fold improvement in photocatalytic activity relative to as-synthesized CdS. The optimum composite retained about 80% of its photocatalytic activity after 15 hours of use.

2. Material and methods

2.1. Materials

All reagents were used as received. Cadmium acetate dihydrate ($Cd(CH_3COO)\cdot 2H_2O$), ammonium molybdate tetrahydrate ($(NH_4)_6Mo_7O_{24}\cdot 4H_2O$), diethylenetriamine or DETA, and lactic acid were purchased from Sigma-Aldrich.

Absolute ethanol was purchased from Merck. Thiourea ($SC(NH_2)_2$) was purchased from Unilab. Standard hydrogen mixture and nitrogen gas were obtained from Linde.

2.2. Cadmium sulfide synthesis

Synthesis of CdS was done via solvothermal reaction at 120 °C using cadmium acetate dihydrate as the cadmium precursor and thiourea as the sulfur precursor with DETA as the solvent. In the preparation process, 1.109 g of cadmium acetate dihydrate and 0.950 g of thiourea (1:3 mol) were added to a 50-ml Teflon-lined stainless-steel autoclave filled with 40 ml of DETA [20]. Water was further added to the mixture for thermal hydrolysis of thiourea producing S^{2-} ions [21]. The mixture was heated in an oven at for 12 hours. After heating, the autoclave was cooled down to room temperature. The yellow precipitates (CdS) were recovered by centrifugation (2500 rpm, 15 min), washing with deionized water and absolute ethanol for several times until pH became neutral, and filtration using a 0.45-µm cellulose membrane filter. The yellow product was then vacuum-dried at 70 °C for 2 h.

2.3. Molybdenum disulfide synthesis

MoS_2 was synthesized via hydrothermal reaction at 200 °C using ammonium molybdate tetrahydrate as the molybdenum precursor and thiourea as the sulfur precursor [22]. Under vigorous stirring (260 rpm, 20 min), 1.236 g of ammonium molybdate tetrahydrate and 1.142 g of thiourea (1:15 mol) were dissolved in a beaker filled with 35 mL deionized water until homogeneity was observed. The solution was transferred to 45-ml Teflon-lined stainless-steel autoclave and heated for 24 h. The system was cooled down to room temperature. The final black product (MoS_2) was recovered via centrifugation (2500 rpm, 15 min), washing with absolute ethanol for several times, and filtration using a 0.45-µm cellulose membrane filter. The product was dried under vacuum at 60 °C for 4 h.

2.4. Composites preparation

Formation of heterojunction between MoS_2 and CdS was done via physical mixing as previously done by Liu et al. using MoS_2 nanosheets and CdS nanorods and originally by Mahler *et al.* using TiO_2 nanopowder and tungsten disulfide (WS_2) nanosheets [22,23]. Initially, as-synthesized MoS_2 was dispersed in hexane (1.3 mg/mL) via ultrasonication for 2.5 min. In an agate mortar under fume hood, 11.54 mL of dispersion (15 mg MoS_2) and 85 mg of as-synthesized CdS were efficiently ground together until air-dry. The ground mixture was then dispersed by the addition of absolute ethanol and then ground again. The composite powder was then dried for 4 h under vacuum at 60 °C. Materials were labelled as: CDS (as-synthesized CdS); MOS (as-synthesized MoS_2); MC05 (5 wt.% of MoS_2 in MoS_2/CdS Composite); MC10 (10 wt.% of MoS_2 in MoS_2/CdS Composite); MC15 (15 wt.% of MoS_2 in MoS_2/CdS Composite); MC20 (20 wt.% of MoS_2 in MoS_2/CdS Composite); and MC25 (25 wt.% of MoS_2 in MoS_2/CdS Composite).

2.5. Characterization

Fourier Transform Infrared (FTIR) absorption spectra of the as-synthesized, ground samples were obtained using Nicolet 6700 FT-IR Spectrometer. Morphological images were obtained from Hitachi Field Emission Scanning Electron Microscope (UHR FE-SEM) SU8230. X-ray fluorescence semi-quantitative analysis of as-synthesized samples was done using handheld X-ray Fluorescence (EDXRF) spectrometer Olympus Innov-X Pro where samples were pressed into a metal container. X-ray Diffraction (XRD) patterns of samples were recorded using Shimadzu Maxima XRD7000 diffractometer with Cu Kα radiation (40.0 kV, 30.0 mA, λ = 1.5406 Å). Each sample were scanned in continuous measurements with Bragg angle ranging from 3° to 90° and a scanning speed of 2° per minute. Ultraviolet-Visible diffuse reflectance spectra of the samples were measured using Lambda 850 UV-Vis Spectrophotometer with an integrating sphere where absolute ethanol was used as medium.

2.6. Photocatalytic activity tests

All batch reactions were carried out in a Pyrex reactor as schematically shown in Figure 1. The photocatalyst with lactic acid solution (10 vol. %) was placed inside the reactor with O-ring seal. The upper part of the reactor consists of ports for the tube used in N_2 purging, the thermocouple, and the septum for gas sampling. The lower part of the reactor, with an internal cylindrical dimension of 5 cm (height) by 5cm (diameter), was where the colloidal system was placed including a polytetrafluoroethylene stir bar. The volume of the headspace where the sample was extracted from was 142 cm^3. Magnetic stirrer (Corning PC-420D) was operated at 300 rpm every run to ensure dispersion. A thermocouple with a sensor was connected to a temperature controller that corrects the operating temperature of the reaction if it exceeds a set value by sending current from supply (Alexan DC Power Supply) to Peltier cell heat exchanger sandwiched with the cold sink and heat sink. The junction between the reactor and the cold sink is a black surface. A 500-W linear halogen lamp (Firefly) was used as the source of irradiation and the visible light was regulated through a UV cut-off filter (Kenko MC UV, >390 nm). The distance between the lamp and the center of the reactor was maintained at 15 cm.

First, 50 mg of the photocatalyst was weighed and placed in the reactor. Subsequently, 10 vol. % lactic acid solution was added, and the mixture was sonicated for 2.5 minutes to initially aid dispersion using ultrasonic cleaner (VGT-800). The upper and lower parts of the glass reactor were sealed with an O-ring and the mixture was purged with nitrogen gas for 15 minutes to eliminate dissolved oxygen in the water. A 0.5-mL sample from the headspace was taken for the initial concentration using a headspace gastight syringe (PALsystem, 2.5 mL). Analyses of headspace composition were done using Gas Chromatograph (Shimadzu GC-2014) with Thermal Conductivity Detector for 3 minutes with a 40-millisecond interval using nitrogen as carrier gas. Subsequent sampling was done every hour for 5 hours. All runs were replicated.

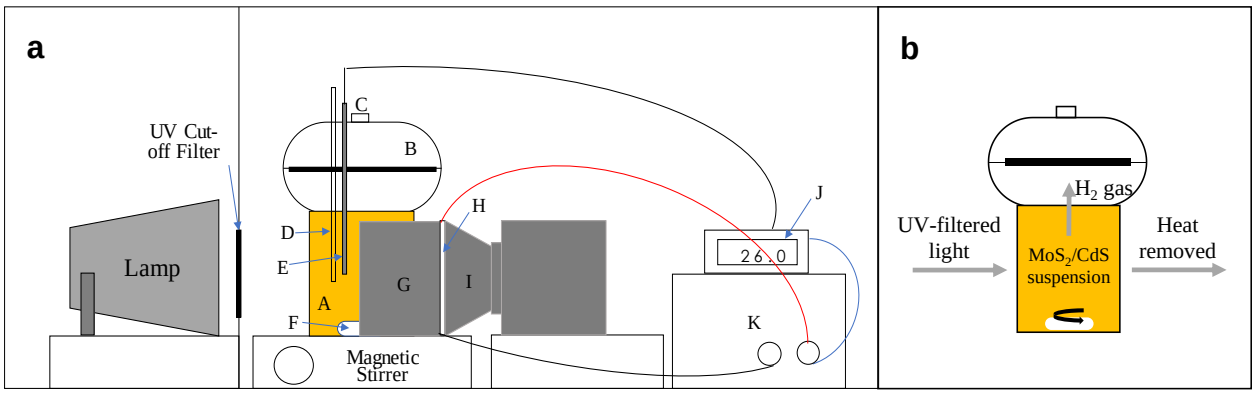

Figure 1 (a) Schematic diagram of the photocatalytic reaction setup and (b) Photocatalytic reaction gas and energy flow. Note that the outer box of this diagram represents a cover against external light source. (A) Glass reactor, (B) Headspace, (C) Sampling port, (D) Glass tube for N_2 purging, (E) Thermocouple, (F) Stir bar, (G) Cold sink, (H) Peltier cell, (I) Heat sink, (J) Temperature controller, (K) Power supply

3. Results and discussion

3.1. Characterizations

Figure 2 shows the as-synthesized samples of (a) CdS and (b) MoS_2 with insets containing their respective semi-quantitative elemental detections using handheld EDXRF spectrometer. Cd and S are detected from the CdS sample with traces of K which was due to the nearness of X-ray energy values of potassium at K shell and of cadmium's Lβ_1. Mo and S are also detected on the as-synthesized MoS_2 sample.

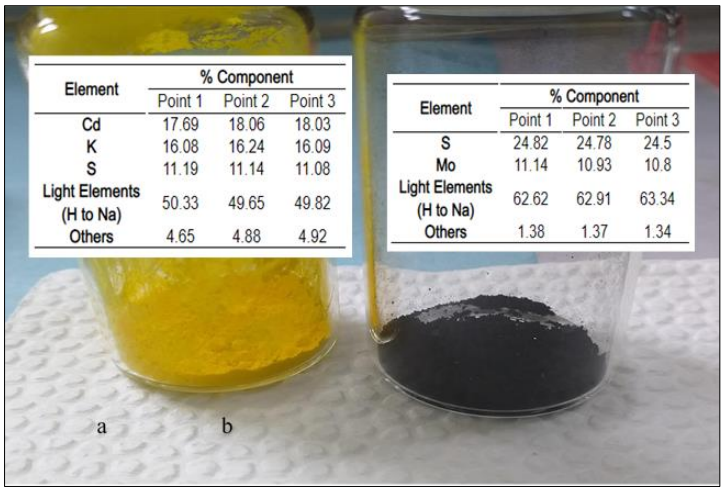

Figure 2 As-synthesized CdS and MoS_2 with EDXRF semi-quantitative detections in the insets

Figure 3 confirms the presence of DETA on CdS-DETA hybrid. The broad peak at around 3300 cm^{-1} is assigned to N-H stretching overlapped by the strong peak of O-H stretching from moisture at around 3400 cm^{-1} while the peak at 1620 cm^{-1} is assigned to N-H bending both from the primary amine group of DETA [24]. The shoulder peak at around 2900 cm^{-1} is assigned to C-H stretching and the weak peak at around 1450 cm^{-1} represents the CH_2 bending [24]. The small

bands from 1000 to 1100 cm^{-1} are that of the C-N stretching [24]. The N-H stretching and bending of the secondary amine for aliphatic compounds are usually unobservable [24]. A narrow peak of stretching vibration of Cd-S can be found at far infrared region at around 615 cm^{-1} [25]. The broad peak observed at far infrared is assigned to out-of-plane N-H bending vibrations. An ionic bond vibration between Mo and S is also detected at 467 cm^{-1} in the spectrum of as-synthesized MoS_2 [26].

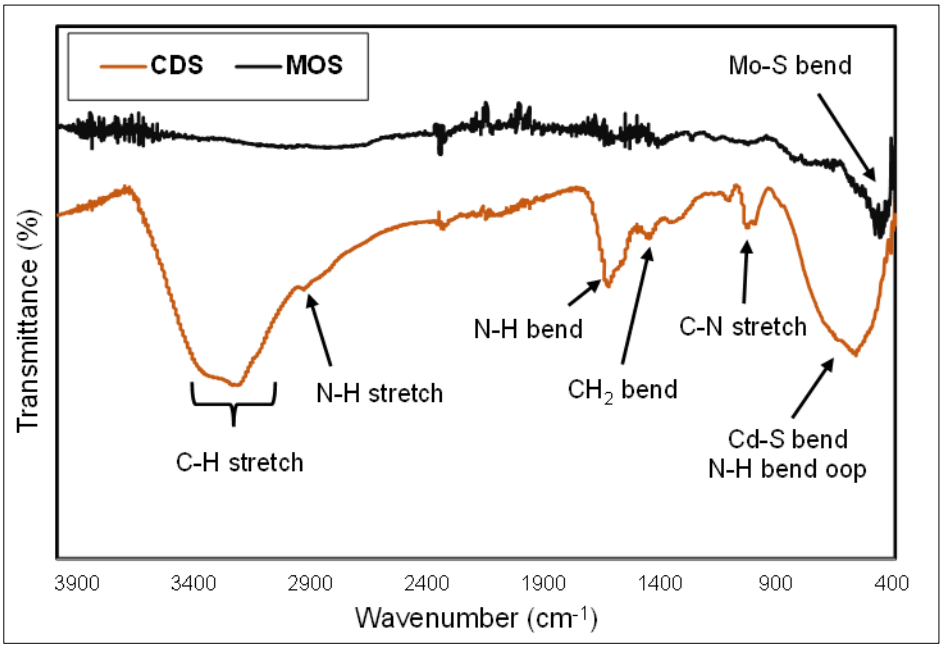

Figure 3 FTIR spectrum of CdS synthesized using solvothermal method (120 °C and 12 h) and MoS_2 using hydrothermal method (200 °C and 24 h)

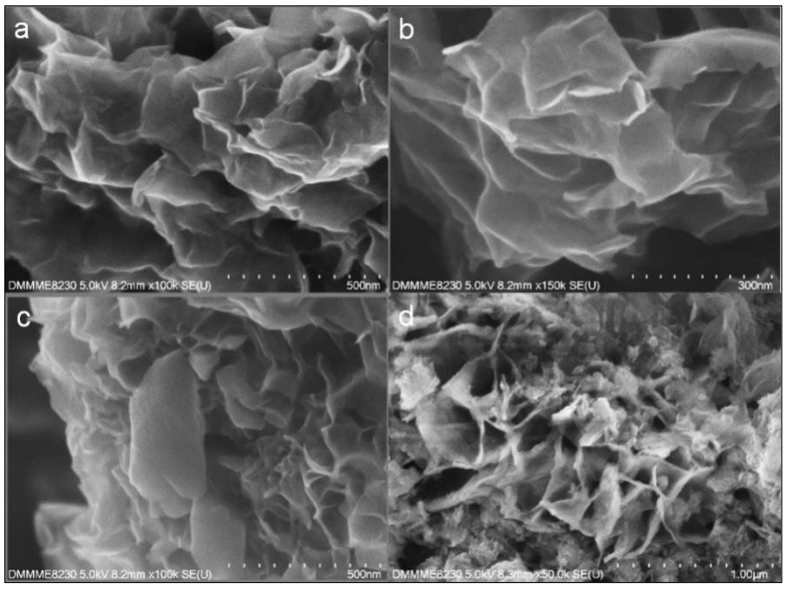

Figure 4 FE-SEM images of (a,b) MoS_2 nanosheets synthesized using hydrothermal method at 200 °C for 24 h, (c) CdS sheets/flakes synthesized using solvothermal method at 120 °C for 12 h, and (d) 15 wt.% MoS_2/CdS composite prepared via grinding

The morphological images of as-synthesized materials are shown in Figure 4. Figures 4a and 4b confirm the 2D sheet-like morphology of MoS_2 with a lateral size of 200-500 nm. The stacking of these nanosheets is typical during the drying process [27]. Successful formation of MoS_2 nanosheets was due to the growth of MoS_2 from precursors with the aid of ammonium ions from their hydrogenated amine groups being intercalated in between layers during the hydrothermal reaction [22]. Figure 4c confirms the 2D sheet-like/flake-like structure of CdS of different sizes (>400 nm lateral). The

formation of such structure was influenced by the presence of diethylenetriamine as reaction solvent particularly due to the surface effects by amine ligands [28]. The microstructure of 15 wt.% composite was shown on Figure 4d. MoS_2 nanosheets (crumpled-paper-like morphology) were successfully adsorbed on the surface of CdS sheets via physical grinding using hexane as solvent for the latter. The fact that MoS_2 has a negative value of zeta potential while CdS has positive, this influenced the effective self-assembly between the two materials to form a composite together with the grinding method [14,29]. Although morphological analysis could not solely suggest heterojunction formation, band gap analysis for the composites and photocatalytic tests for a synergistic effect should be performed.

The peaks at 13.9°, 33.6°, 39.7°, and 59.1° in Figure 5 corresponds respectively to (002), (100), (103), and (110) planes of the hexagonal crystal structure of MoS_2 and were consistent with that of several studies using Joint Committee on Powder Diffraction Standards (JCPDS) number 37-1492 as reference [30-32]. The peak location of (002) plane and its interlayer spacing are substantially similar with that of 1T-MoS_2 synthesized by Mishra *et al.* [33]. Similar peaks were observed in the as prepared MoS_2 of Ding *et al.* with 24.7% 1T phase using the same precursors of this work operated at 210 °C for approximately 19 hours [30]. Similar peaks could also be observed on the study of Liu *et al.* where they synthesized 12-16% 1T-MoS_2 using Na_2MoO_4 and $(NH_4)_2MoS_4$ as molybdenum precursor and thiourea as sulfur precursor in a hydrothermal reaction operated at 200 °C for 24 hours [34]. The *d*-spacing values or the distance between planes of atoms of planes Mo-Mo (100) were close to reported values taken from TEM images and XRD patterns for 1T-MoS_2 which would be around 3.15-3.18 Å for pure 2H-MoS_2 [22,33,35]. Typical values of *d*-spacing for (002) plane of 2H phase MoS_2 were around 6.1-6.2 Å [29,30,36]. In this work, the as-synthesized MoS_2 nanosheets had larger *d*-spacing value for (002) plane which means some parts of MoS_2 were successfully intercalated with ammonium ions, which altered its trigonal prismatic phase to an octahedral one. This analysis was also observed in the study of Kim *et al.* using Li ions as intercalant where the interlayer spacing of pristine 2H MoS_2 was increased from 6.08 Å to 6.14 Å after intercalation and the peak for (002) which was around 14.38°-14.40° shifted to a lower degree when it was intercalated [37]. Moreover, similar observations were made by several studies on intercalation of MoS_2 [27,38,39]. This means that the as-synthesized MoS_2 nanosheets undergone incomplete chemical exfoliation where 1T phase and 2H phase both occurred in the material. The presence of 2H phase is not ultimately unfavorable. It contributes to the stability of the material during storage, handling such as in composite preparation, and application. Using JCPDS 01-077-2306, the peaks of CdS pattern at 25.8°, 27.0°, 28.7°, 37.2°, 44.2°, 48.4°, and 52.3° were indexed respectively as (100), (002), (101), (102), (110), (103), and (112) planes of hexagonal phase of CdS. Similar peaks for CdS were observed by past studies [20,38,46]. The strong peak at (002) indicates high crystallinity of CdS sheets with preferred growth along that plane. The interlayer spacing along this plane (0.330 nm) was consistent with the TEM images of other studies of hexagonal CdS [20,19,52].

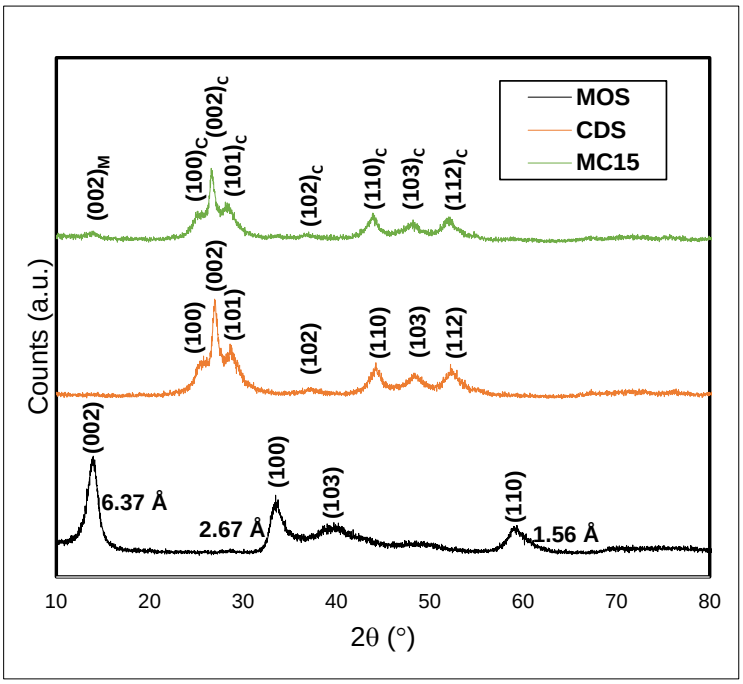

Figure 5 XRD pattern of MoS_2 nanosheets synthesized using hydrothermal method at 200 °C for 24 h, CdS sheets synthesized using solvothermal method at 120 °C for 12 h and 15 wt.% MoS_2/CdS composite prepared via grinding. (Note: "M" is subscript for MoS_2 and "C" for CdS.)

Obtaining hexagonal crystal structure of CdS rather than cubic phase alone contributes to the photocatalytic activity since the former has a narrower band gap [41,42]. Other than the morphological similarity of MoS_2 and CdS, it would also be significant that their crystalline structures are also similar. It contributes to the quality of their heterojunction promoting electron-hole pair separation and further inhibits photocorrosion of CdS [15]. Based on their crystalline structures, it is expected that hydrogen evolution will be enhanced. The XRD pattern for 15 wt.% MoS_2/CdS composite was also recorded. The crystallinity of CdS sheets was sustained even after the composite preparation. A small peak at 13.89° was that of (002) plane of MoS_2 as discussed earlier. Furthermore, the *d*-spacing of MoS_2 nanosheets at *c*-axis was unchanged. This means that the physical grinding method including the dispersion on hexane via ultrasonication (2.5 min) did not affect the crystallinity of MoS_2 nanosheets.

Table 1 summarizes the *c*-stacking height of as-synthesized composite precursors. Using Scherrer equation, the estimated *c*-stacking height of MoS_2 nanosheets was about 6 nm. Chang *et al.* reported the enhancement effect of the thinness of MoS_2 on the hydrogen evolution and confirmed the dependence of catalytic properties on particle size [13]. The approximate *c*-stacking height of CdS sheets along (002) plane was about 9 nm. This would enhance the photocatalytic activity of CdS due to higher electron mobility of thinner materials which could further restrain the electron-hole pair recombination in the case of CdS.

Table 1 Approximate values of *c*-stacking height and number of layers for as-synthesized MoS_2 and CdS from their diffraction data using Scherrer method

Sample	2θ (°)	Bragg Angle (°)	FWHM (°)	c-Stacking Height (nm)	Interlayer spacing (nm)	Number of layers
MOS	13.88	6.94	1.304	6.14	0.6374	11
CDS	27.04	13.52	0.965	8.47	0.3295	27

As-synthesized CdS sheets, MoS_2 nanosheets, and their composites were characterized using UV-Vis diffused reflectance spectroscopy. Figure 6a shows the characteristic absorption edge of CdS at 500-510 nm [36,43,47]. Enhancement of absorption in the visible region (500-800 nm) with increased dosage of MoS_2 on CdS was due to the dark color of the former.

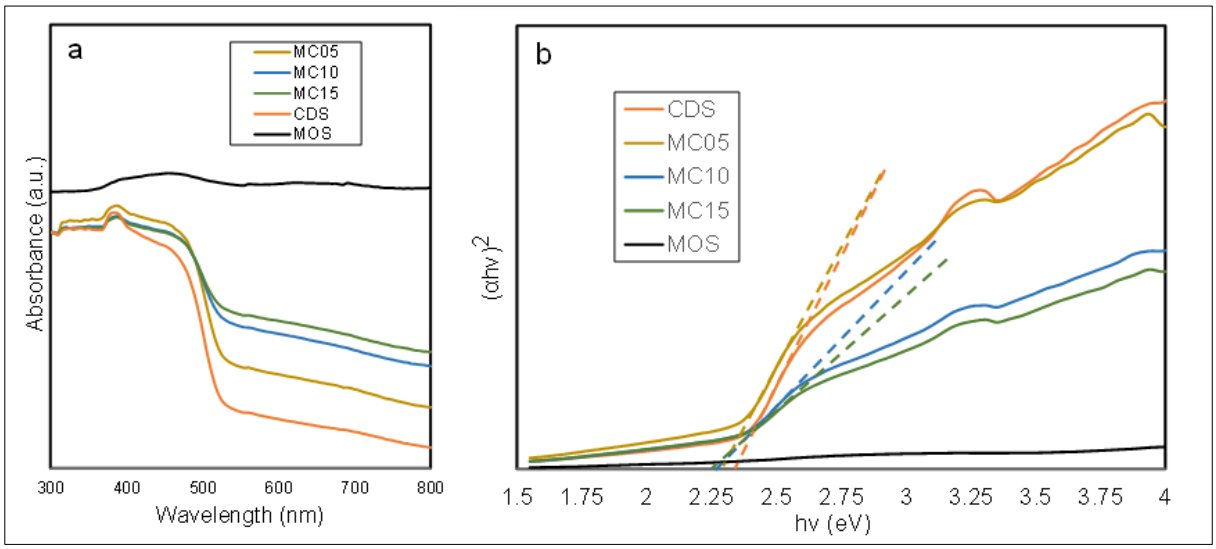

Figure 6 (a) UV-Vis Diffuse Reflectance Spectra of CdS, MoS_2, 5 wt.% MoS_2/CdS, 10 wt.% MoS_2/CdS, and 15 wt.% MoS_2/CdS and (b) their corresponding Tauc plots

The band gap energies of CdS and composites were estimated using Tauc plots $(\alpha hv)^n$ versus hv using the equation: $(\alpha hv)^n = A(hv - E_g)$ where α is the absorption coefficient, hv is the photonic energy or the product of Planck constant and frequency (speed of light per wavelength), A is a constant, E_g is the band gap energy, and n is equal to 2 for direct band gap and 1/2 for indirect. The value of α is calculated using the absorbance from diffuse reflectance spectra over the thickness of particle in cm, and hv in eV is equal to $1240/\lambda$ where λ is in nm. To calculate for E_g from the equation above,

α must be set to zero (y-axis will become zero). A line was extrapolated from Tauc plot's steepest linear part to the x-axis as shown in Figure 6b. The thickness of the particle was set to 10 nm for all the samples close to the approximated value of c-stacking height for CdS sheets. Summary of band gap values was shown in Table 2. The band gap of CdS was close to the reported values, 2.25-2.40 eV [13,36,44]. The presence of MoS_2 on CdS did not significantly affect the direct band gap of CdS. These results were an indication that MoS_2 was successfully deposited on CdS surface and did not intervene into its lattice structure. The band gap values of CdS and its composites with MoS_2 were sufficient for water splitting to proceed forwardly with a free energy requirement of 1.23 eV.

Table 2 Direct band gaps of CdS sheets synthesized via solvothermal method at 120 °C for 12 h, MoS_2 nanosheets synthesized using hydrothermal method at 200 °C for 24 h and different composites prepared via grinding

Sample	Band Gap (eV)
CDS	2.32
MC05	2.30
MC10	2.28
MC15	2.27
MOS	1.76

3.2. Photocatalytic activity

Batch-reaction photocatalytic tests were performed using different photocatalysts dispersed in water for 5 hours under visible light irradiation ($\lambda > 390$ nm) in the presence lactic acid as hole scavenger. Linear halogen lamp (Firefly, 500 W) was used as the light source. Temperature was maintained at 27±2 °C. All photocatalytic runs were replicated. Three samples of the headspace were obtained per GC analysis every hour using a gas-tight syringe. As shown in Figure 7a, all materials exhibited a linear plot when hydrogen evolution was plotted against time confirming the zero-order reaction in a span of 5 hours. Figure 7b shows that control experiments exhibited insignificant rate of hydrogen evolution. Pristine MoS_2 nanosheets were initially tested for photocatalytic activity under direct sunlight irradiation for 4 hours in water. The chromatogram in Figure S1 recorded the absence of hydrogen gas whose peak must be located at around 0.9-1.0 minute's retention time. Using Tauc method, the direct band gap energy of MoS_2 (2H) was estimated to be 1.76 eV (See Table 2) which was close to earlier reports [45,46]. Although theoretically this value would be sufficient for water splitting reaction to proceed which only needs 1.23 eV potential difference, an ideal band gap for a photocatalyst must be between 2.0 to 2.2 eV to overcome inherent charge transfer energy losses [3]. Moreover, in the case of metallic MoS_2 (1T), it does not have a band gap, therefore, its HER photocatalytic activity is unappreciable. CdS sheets alone, on the other hand, exhibited poor activity of 6.5 μmol g_{cat}^{-1} h^{-1} which was due to its innate rapid electron-hole pair recombination property—the reason why CdS with cocatalyst that promotes hydrogen adsorption and reduction is necessary. Composite MC15 with 15 wt.% MoS_2 exhibited the maximum hydrogen evolved (1036.1 μmol g_{cat}^{-1} h^{-1}) which enhanced the photocatalytic activity of bare CdS by 159 times. Beyond a dosage of 15 wt.% MoS_2 nanosheets, the rate of hydrogen production decreased. This can be explained by the shielding effect of the excess amount of MoS_2 nanosheets blocking and absorbing the visible light irradiation that could have been utilized by CdS [18,29]. The optimum loading of 15 wt.% is close to the reported values of optimum loading of inhomogeneous MoS_2 on CdS in other studies. The composite with 10wt% inhomogeneous MoS_2 on CdS nanorods from the study of Liu *et al.* exhibited superior photocatalytic activity compared to 5 wt.% and 20 wt.% composites [22]. Furthermore, among five loadings, Du *et al.* recorded an optimum loading of 10wt% MoS_2 on CdS nanorods followed by 20 wt.% loading in terms of photocatalytic activity [43]. The enhanced performance of the composites indicates that heterojunctions between MoS_2 and CdS were formed through which photoexcited electrons from CdS transfer across to MoS_2.

The synergistic effect on the photocatalytic activity observed in this study is superior compared to most of the recent studies using similar composites in terms of enhancement as shown in Table 3. Furthermore, the 159-fold enhancement is comparable to the 167-fold enhancement from the study of Yin *et al.* using MoS_2/CdS nanosheet-on-nanorod [51]. The huge enhancement was due to the substantial suppression of photogenerated electron-hole pair recombination caused by: (1) The morphological similarity of MoS_2 nanosheets and CdS sheets/flakes forming face contact as shown in their FE-SEM images; (2) The hexagonal crystal structure of CdS and its similarity with that of the 2H component of MoS_2 as indicated on their XRD patterns making the heterojunction between them more intimate; (3) The enhanced HER activity of MoS_2 nanosheets containing metallic phase; (4) The thinness of MoS_2 nanosheets and CdS sheets/flakes; and (5) The presence of lactic acid as hole scavenger.

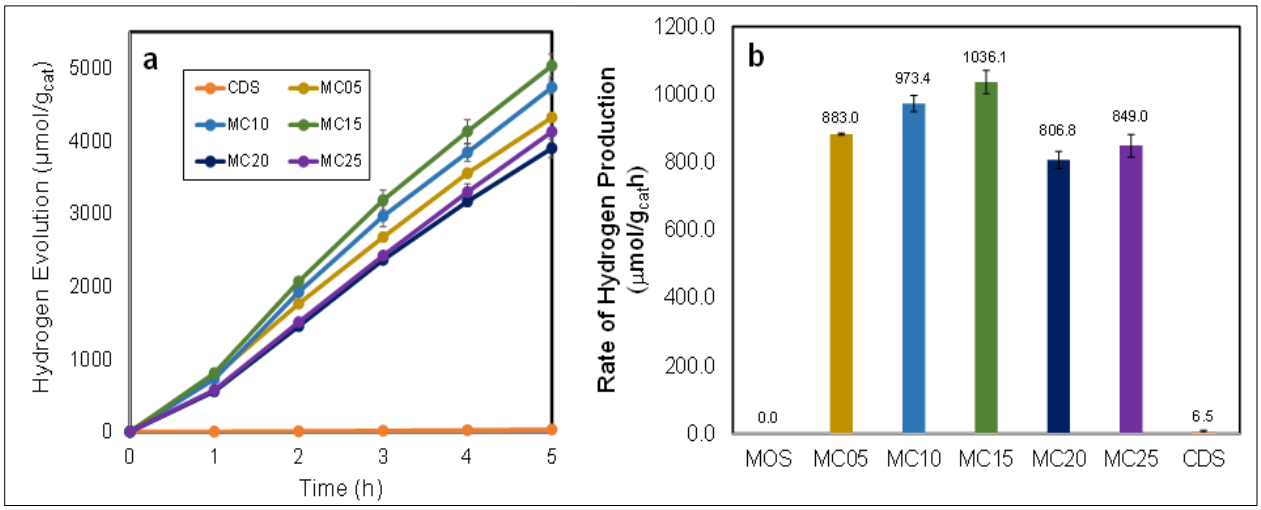

Figure 7 (a) Hydrogen evolution throughout the 5-hour run and (b) summary of rates of hydrogen production performed under visible light (λ > 390 nm) irradiation using lactic acid as sacrificial agent

Table 3 Photocatalytic activity comparison of recently reported MoS_2/CdS composite photocatalysts

Photocatalyst	**Mass (mg)**	**Light Source**	**Sacrificial Agent**	**H_2 Production Rate (mmol g_{cat}^{-1} h^{-1})**	**Enhancement rel. to bare CdS**	**Ref.**
Lamellar flower-like MoS_2 on CdS	3	300 W Xe Lamp (λ ≥ 420 nm)	10 vol % Lactic acid	54.1	36	[16]
2D-2D MoS_2/CdS	50	300 W Xe Lamp (λ ≥ 400 nm)	0.5 mol L^{-1} of Na_2S–Na_2SO_3	1.75	2	[18]
2D-2D MoS_2/CdS	50	300 W Xe Lamp (λ ≥ 420 nm)	0.4 mol L^{-1} of Na_2S–Na_2SO_3	26.32	34	[19]
Nanosheets-on-nanorods MoS_2/CdS	20	300 W Xe Lamp (λ ≥ 420 nm)	10 vol % Lactic acid	39.75	35	[43]
Cauliflower-like morphology	100	300 W Xe Lamp (λ ≥ 400 nm)	10 vol % Lactic acid	4.1	17	[44]
Nanodots-on-nanorods MoS_2/CdS	2	500 W Metal Halide Lamp (λ ≥ 420 nm)	10 vol % Lactic acid	131.7	66	[45]
Nanospherical MoS_2/CdS	50	300 W Xe Lamp (λ ≥ 400 nm)	10 vol % Triethanolamine	2.48	50	[47]
Nanosheets-on-nanorods MoS_2/CdS	50	300 W Xe Lamp (λ ≥ 420 nm)	16.7 vol % Lactic acid	10.84	6	[48]
Nanosheets-on-nanorods MoS_2/CdS	20	300 W Xe Lamp (λ ≥ 420 nm)	Lactic acid	45.2	167	[51]
2D-2D MoS_2/CdS	50	500 W Halogen Lamp (λ ≥ 390 nm)	10 vol % Lactic acid	1.04	159	This work

The enhanced photocatalytic hydrogen production of the composites confirms the synergistic effect between MoS_2 and CdS in the presence of lactic acid where CdS acts as the photoactive material capable of absorbing energy from visible light (λ > 390 nm) and using this photonic energy to excite its electron from the valence band to the conduction band. The apparent enhanced photocatalytic activity in the presence of MoS_2 on CdS can be explained by the efficient

consumption of electron-hole pairs upon photoexcitation. As shown in Figure 8, these photoexcited electrons, through the heterojunction formed, travelled to the locations where H atoms are adsorbed, namely, the active sites of 2H-MoS_2 mainly found on its edges and of 1T-MoS_2 found on its basal plane and edges [14]. Holes were scavenged by lactic acid while the electrons were consumed by the adsorbed H atoms on the MoS_2 surface with active sites to form hydrogen gas.

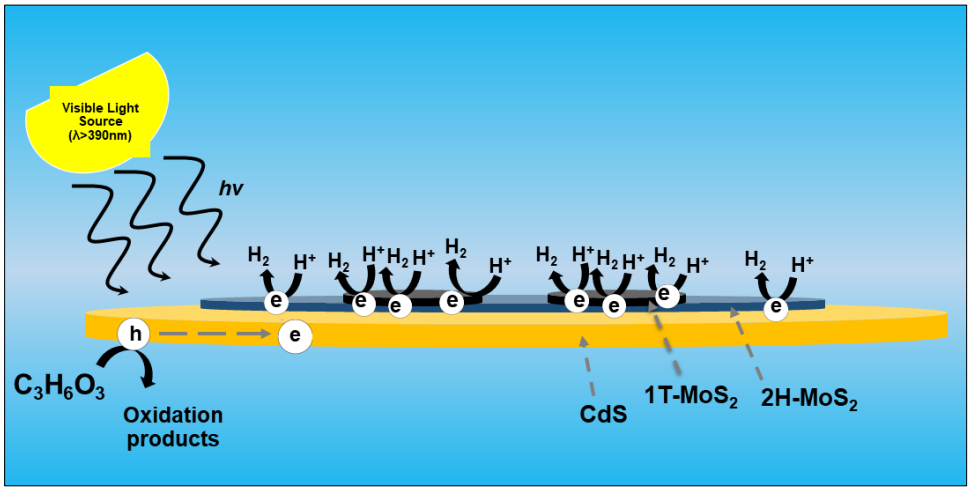

Figure 8 Proposed schematic diagram of the photocatalytic reaction

3.3. Stability test

The stability of the photocatalyst was assessed through a 3-cycle photocatalytic run. Each cycle was a 5-hour visible light irradiation and was done on consecutive days. After the cycle, the photocatalyst stayed in the reaction system for 24 hours to be reused for the next cycle. The reaction system was purged with fresh nitrogen gas for 20 minutes to evacuate hydrogen before every cycle. Figure 9 shows the slight degradation of the photocatalytic activity of 15 wt.% MoS_2/CdS. During the first cycle, the composite generated hydrogen at a rate of 1007.4 μmol g_{cat}^{-1} h^{-1}. After 15 hours with two sets of deactivation-activation, approximately 80 % of activity was still achieved. Photocorrosion of metal sulfide through time plays a role in the decline of the photocatalyst's activity [49]. The degradation of this composite photocatalyst's activity is due to falling off of some MoS_2 nanosheets [18,50].

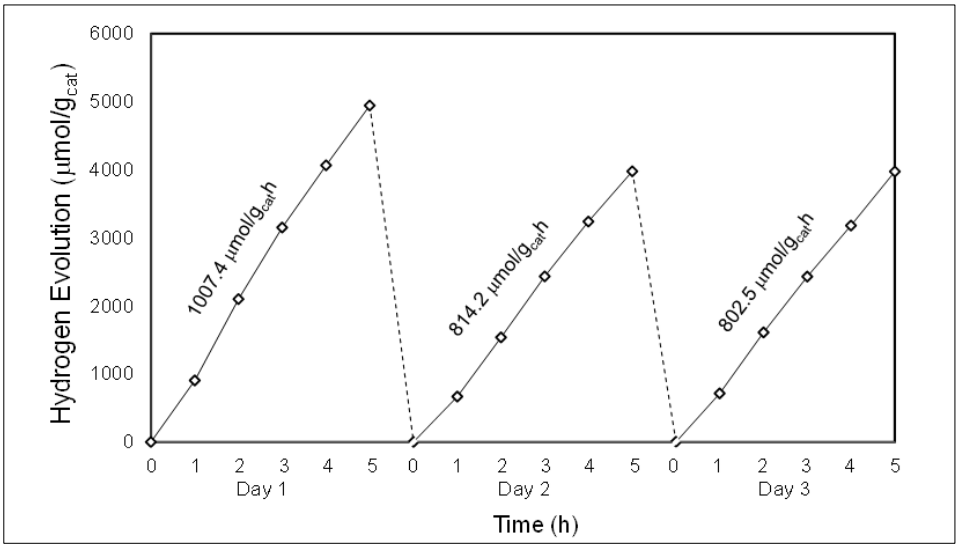

Figure 9 Stability test of 15 wt.% MoS_2/CdS via 3 cyclic runs under visible light (λ > 390 nm) irradiation using lactic acid as sacrificial agent

4. Conclusion

In this study, composites of phase inhomogeneous MoS_2 nanosheets and CdS sheets/flakes were synthesized and tested for hydrogen evolution reaction under visible light irradiation using lactic acid as sacrificial agent. The XRD pattern of MoS_2 nanosheets synthesized using a hydrothermal method confirmed both its 1T and 2H phases and its hexagonal crystal structure while its XRF semi-quantitative data and FTIR spectrum verified the presence of Mo and S atoms. CdS sheets/flakes synthesized from a solvothermal method was shown to have a hexagonal crystal structure as confirmed by its XRD pattern while its XRF semi-quantitative data verified the presence of Cd and S atoms. CdS, including its synthesis solvent that influenced its sheet-like morphology was detected by its FTIR absorption spectrum while its characteristic band edge was confirmed by its UV-Vis absorption spectrum. Using Scherrer's equation, both as-synthesized MoS_2 nanosheets and CdS sheets were proven to be few-layered. The FE-SEM image of MoS_2/CdS composite synthesized using physical mixing confirmed the adsorption of MoS_2 nanosheets on CdS sheets/flakes. The XRD patterns of 15 wt.% composite confirmed the preservation of the crystal structures of both materials after the preparation procedure. Using Tauc method from UV-Vis Diffuse Reflectance Spectroscopy, the band gaps of CdS and the composites were substantially unchanged indicating successful adsorption of MoS_2 on CdS. An apparent synergistic effect of the two materials was observed having an optimum hydrogen production rate of 1036.1 μmol g_{cat}^{-1} h^{-1} for the 15 wt.% MoS_2/CdS composite which was 159 times larger than bare CdS. The optimum composite retained about 80% of its photocatalytic activity after 15 hours of use.

Compliance with ethical standards

Acknowledgments

Financial support from the Engineering Research and Development for Technology (ERDT) program of the Department of Science and Technology – Science Education Institute is acknowledged.

Disclosure of conflict of interest

The authors of this paper have no conflicts of interest to disclose.

References

[1] C. Acar, I. Dincer, and G. F. Naterer, "Review of photocatalytic water-splitting methods for sustainable hydrogen production," Int. J. energy Res., 2016.

[2] I. Dincer and C. Acar, "Review and evaluation of hydrogen production methods for better sustainability," Int. J. Hydrogen Energy, vol. 40, no. 34, pp. 11094–11111, 2014.

[3] R. M. Navarro, Yerga, M. C. Alvarez-Galván, F. Vaquero, J. Arenales, and J. L. G. Fierro, "Hydrogen production from Water Splitting Using Photo-Semiconductor Catalysts," Renew. Hydrog. Technol. Prod. Purification, Storage, Appl. Saf., pp. 43–61, 2013.

[4] A. Fujishima and K. Honda, "Electrochemical photolysis of water one and two-dimensional structure of poly (L-Alanine) shown by specific heat measurements at low," Nature, vol. 238, pp. 37–38, 1972.

[5] Y. Ohko, K. Hashimoto, and A. Fujishima, "Kinetics of photocatalytic reactions under extremely low-intensity UV illumination on titanium dioxide thin films," J. Phys. Chem. A, vol. 101, no. 43, pp. 8057–8062, 1997.

[6] H. Yan, X. Wang, M. Yao, and X. Yao, "Band structure design of semiconductors for enhanced photocatalytic activity: The case of TiO_2," Prog. Nat. Sci. Mater. Int., vol. 23, no. 4, pp. 402–407, 2013.

[7] Y. Xu and M. A. A. Schoonen, "The absolute energy positions of conduction and valence bands of selected semiconducting minerals," Am. Mineral., vol. 85, pp. 543–556, 2000.

[8] S. Wang, B. Zhu, M. Liu, L. Zhang, J. Yu, and M. Zhou, "Direct Z-scheme ZnO/CdS hierarchical photocatalyst for enhanced photocatalytic H_2-production activity," Appl. Catal. B Environ., vol. 243, pp. 19–26, 2019.

[9] A. Meng, B. Zhu, B. Zhong, L. Zhang, and B. Cheng, "Direct Z-scheme TiO_2/CdS hierarchical photocatalyst for enhanced photocatalytic H_2-production activity," Appl. Surf. Sci., vol. 422, pp. 518–527, 2017.

[10] J. Liu, D. Zhang, X. Pu, J. Liu, and R. Zhang, "Combustion synthesis of $Zn_{1-x}Cd_xS$ and its photodegradation performance of methylene blue," Mater. Lett., vol. 117, pp. 158–161, 2014.

[11] K. Wu, H. Zhu, Z. Liu, W. Rodríguez-Córdoba, and T. Lian, "Ultrafast charge separation and long-lived charge separated state in photocatalytic CdS-Pt nanorod heterostructures," J. Am. Chem. Soc., vol. 134, no. 25, pp. 10337–10340, 2012.

[12] M. Chhowalla, H. S. Shin, G. Eda, L. J. Li, K. P. Loh, and H. Zhang, "The chemistry of two-dimensional layered transition metal dichalcogenide nanosheets," Nat. Chem., vol. 5, no. 4, pp. 263–275, 2013.

[13] K. Chang *et al.*, "Drastic layer-number-dependent activity enhancement in photocatalytic H_2 evolution over n MoS_2/CdS (n ≥ 1) under visible light," vol. 201402279, 2015.

[14] D. Voiry *et al.*, "Conducting MoS_2 nanosheets as catalysts for hydrogen evolution reaction," Nano Lett., vol. 13, no. 12, pp. 6222–7, 2013.

[15] E. Cui, G. Yu, H. Huang, and Z. Li, "Current advances in MoS_2/semiconductor heterojunction with enhanced photocatalytic activity," Curr. Opin. Green Sustain. Chem., vol. 6, pp. 42–47, 2017.

[16] L. Su, L. Luo, J. Wang, T. Song., W. Tu, and Z. Wang, "Lamellar flower-like porous MoS_2 as an efficient cocatalyst to boost photocatalytic hydrogen evolution of CdS," Catal. Sci. Technol., vol. 11, pp. 1292-1297, 2020.

[17] J. Low, S. Cao, J. Yu, and S. Wageh, "Two-dimensional layered composite photocatalysts," Chem. Commun., vol. 50, no. 74, pp. 10768–10777, 2014.

[18] S. Ma *et al.*, "Constructing 2D layered hybrid CdS nanosheets/MoS_2 heterojunctions for enhanced visible-light photocatalytic H_2 generation," Appl. Surf. Sci., vol. 391, pp. 580–591, 2017.

[19] Y. J. Yuan *et al.*, "Role of two-dimensional nanointerfaces in enhancing the photocatalytic performance of 2D-2D MoS_2/CdS photocatalysts for H_2 production," Chem. Eng. J., vol. 350, no. April, pp. 335–343, 2018.

[20] F. Vaquero, R. M. Navarro, and J. L. G. Fierro, "Influence of the solvent on the structure, morphology and performance for H_2 evolution of CdS photocatalysts prepared by solvothermal method," Appl. Catal. B Environ., vol. 203, pp. 753–767, 2017.

[21] F. Vaquero, J. L. G. Fierro, and R. M. N. Yerga, "From nanorods to nanowires of CdS synthesized by a solvothermal method: Influence of the morphology on the photoactivity for hydrogen evolution from water," Molecules, vol. 21, no. 4. 2016.

[22] Q. Liu *et al.*, "Gram-scale aqueous synthesis of stable few-layered 1T-MoS_2: Applications for visible-light-driven photocatalytic hydrogen evolution," Small, vol. 11, no. 41, pp. 5556–5564, 2015.

[23] B. Mahler, V. Hoepfner, K. Liao, and G. A. Ozin, "Colloidal synthesis of 1T-WS_2 and 2H-WS_2 nanosheets: Applications for photocatalytic hydrogen evolution," J. Am. Chem. Soc., vol. 136, no. 40, pp. 14121–14127, 2014.

[24] D. L. Pavia, G. M. Lampman, and G. S. Kriz, "Introduction to spectroscopy (3rd Ed.)." Thomson Learning, Inc., 2001.

[25] N. Santhosh Kumar, D. Govinda, and G. Thirumala Rao, "Synthesis, structural and morphological studies of CdS nanopowder," Int. J. Chem. Sci., vol. 15, no. 1, pp. 409–414, 2017.

[26] P. Ramos, I. Coppel, M. Avella, and Jesus G. "α- MoO_3 crystals with a multilayer stack structure obtained by annealing from a lamellar MoS_2/g-C_3N_4 nanohybrid," Nanomaterials, vol. 8, no. 559, 2018.

[27] X. Geng *et al.*, "Two-dimensional water-coupled metallic MoS_2 with nanochannels for ultrafast supercapacitor," Nano Lett., 17, 1825–1832, 2017.

[28] Y. Xu, W. Zhao, R. Xu, Y. Shi, and B. Zhang, "Synthesis of ultrathin CdS nanosheets as efficient visible-light-driven water splitting photocatalysts for hydrogen evolution," R. Chem. Soc., 2013.

[29] X. Li, X. Lv, N. Li, J. Wu, Y. Zheng, and X. Tao, "One-step hydrothermal synthesis of high-percentage 1T-phase MoS2 quantum dots for remarkably enhanced visible-light-driven photocatalytic H_2 evolution," Appl. Catal. B Environ., vol. 243, no. October 2018, pp. 76–85, 2019.

[30] W. Ding *et al.*, "Highly ambient-stable 1T-MoS_2 and 1T-WS_2 by hydrothermal synthesis under high magnetic fields," ACS Nano, vol. 13, pp. 1694–1702, 2019.

[31] W. Jia, X. Zhou, Y. Huang, Y. Cao, Y. Sun, and D. Jia, "Synthesis of air-stable 1T phase of molybdenum disulfide for efficient electrocatalytic hydrogen evolution," 2019.

[32] S. V. P. Vattikuti and C. Byon, "Synthesis and characterization of molybdenum disulfide nanoflowers and nanosheets: Nanotribology," J. Nanomater., vol. 2015, no. c, 2015.

[33] R. K. Mishra, S. Manivannan, K. Kim, H. I. Kwon, and S. H. Jin, "Petal-like MoS_2 nanostructures with metallic 1T phase for high performance supercapacitors," Curr. Appl. Phys., vol. 18, no. 3, pp. 345–352, 2018.

[34] Y. Liu, Y. Xie, L. Liu, and J. Jiao, "Sulfur vacancy induced high performance for photocatalytic H_2 production over 1T@2H phase MoS2 nanolayers," Catal. Sci. Technol., vol. 7, no. 23, pp. 5635–5643, 2017.

[35] S. S. Chou *et al.*, "Controlling the metal to semiconductor transition of MoS_2 and WS_2 in solution," J. Am. Chem. Soc., vol. 137, no. 5, pp. 1742–1745, 2015.

[36] K. Chang, Z. Mei, T. Wang, Q. Kang, S. Ouyang, and J. Ye, "MoS_2/graphene cocatalyst for efficient photocatalytic H_2 evolution under visible light irradiation," ACS Nano, vol. 8, no. 7, pp. 7078–7087, 2014.

[37] J. S. Kim *et al.*, "Electrical transport properties of polymorphic MoS_2," ACS Nano, vol. 10, no. 8, pp. 7500–7506, 2016.

[38] N. Thi Xuyen and J. M. Ting, "Hybridized 1T/2H MoS_2 having controlled 1T concentrations and its use in supercapacitors," Chem. - A Eur. J., vol. 23, no. 68, pp. 17348–17355, 2017.

[39] J. Zheng et al., "High yield exfoliation of two-dimensional chalcogenides using sodium naphthalenide," Nat. Commun., vol. 5, pp. 1–7, 2014.

[40] Q. Gai *et al.*, "2D-2D heterostructured CdS–CoP photocatalysts for efficient H_2 evolution under visible light irradiation," Int. J. Hydrogen Energy, vol. 44, pp. 27412–27420, 2019.

[41] X. Yang, B. Wang, Y. Mu, M. Zheng, and Y. Wang, "Photocatalytic performance of cubic and hexagonal phase CdS synthesized via different Cd sources," J. Electron. Mater., 2019.

[42] M. Matsumura, S. Furukawa, Y. Saho, and H. Tsubomura, "Cadmium sulfide photocatalyzed hydrogen production from aqueous solutions of sulfite: Effect of crystal structure and preparation method of the catalyst," J. Phys. Chem., vol. 89, no. 8, pp. 1327–1329, 1985.

[43] P. Du, Y. Zhu, J. Zhang, D. Xu, W. Peng, and G. Zhang, "Metallic 1T phase MoS_2 nanosheets as a highly efficient co-catalyst for the photocatalytic hydrogen evolution of CdS nanorods," RSC Adv., vol. 6, pp. 74394–74399, 2016.

[44] J. Xu and X. Cao, "Characterization and mechanism of MoS_2/CdS composite photocatalyst used for hydrogen production from water splitting under visible light," Chem. Eng. J., vol. 260, pp. 642–648, 2015.

[45] L. Li, X. Yin, and Y. Sun, "Facile synthesized low-cost MoS_2/CdS nanodots-on-nanorods heterostructures for highly efficient pollution degradation under visible-light irradiation," Sep. Purif. Technol., vol. 212, no. November 2018, pp. 135–141, 2019.

[46] S. Umrao, J. Jeon, S. M. Jeon, Y. J. Choi, and S. Lee, "A homogeneous atomic layer $MoS_{2(1-x)}Se_{2x}$ alloy prepared by low-pressure chemical vapor deposition, and its properties," Nanoscale, vol. 9, no. 2, pp. 594–603, 2017.

[47] X. Jin and G. Li, "Synthesis of MoS_2/CdS nanospheres enhanced photocatalytic hydrogen evolution under visible light," Journal of Materials Science: Materials in Electronics, vol. 31, pp. 9377-9384, 2020.

[48] W.Chen, X.Liu, S.Wei, Q.Heng, B.Want, S.Liu, L. Gao, and L. Mao, "In situ growth of a-few-layered MoS_2 on CdS nanorod for high efficient photocatalytic H_2 production," Frontiers in Energy, vol. 15, pp. 752-759, 2021.

[49] J. He *et al.*, "CdS nanowires decorated with ultrathin MoS_2 nanosheets as an efficient photocatalyst for hydrogen evolution," ChemSusChem, vol. 9, no. 6, pp. 624–630, 2016.

[50] G. Bi *et al.*, "Efficient visible-light photocatalytic H_2 evolution over metal-free g-C_3N_4 co-modified with robust acetylene black and $Ni(OH)_2$ as dual co-catalysts," RSC Adv., vol. 6, no. 37, pp. 31497–31506, 2016.

[51] X. Yin, L. Li, Y. Wang, L. Yao, X. Li, and Y. Lu. "MoS_2/CdS nanosheet-on-nanorod: An efficient photocatalyst for H_2 generation from lactic acid decomposition," Int J Hydrogen Energy, vol. 47, pp. 20103-20111, 2022

Supplementary Material

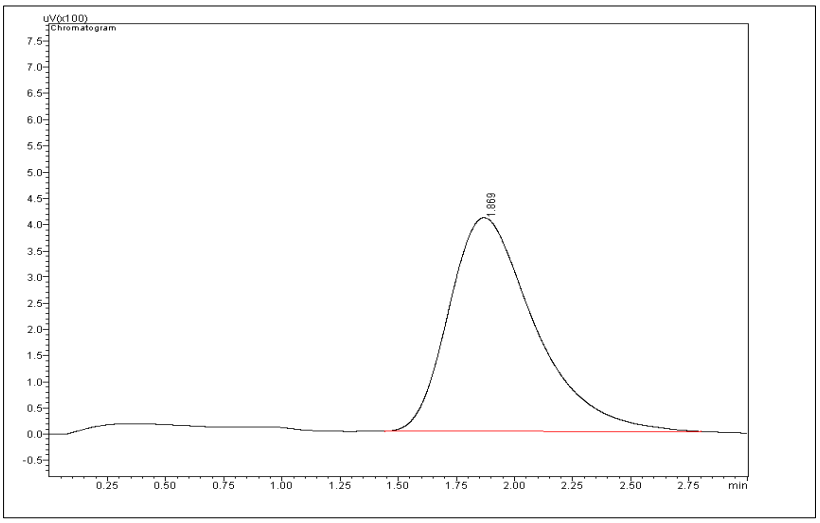

Figure S1 Headspace chromatogram of a photocatalytic system using MoS_2 nanosheets exposed under direct sunlight irradiation for 4 hours